International Journal of Scientific Engineering and Applied Science (IJSEAS) - Volume-1, Issue-9,December 2015

ISSN: 2395-3470

www.ijseas.com

Integrated Energy Management for a Wind–Diesel–Hydrogen-Based Remote Area Power Supply System to Meet Fluctuating Load Using Neural Networks

[1]T.VIGNESH, [2]G.BOOPATHIRAJ

[1]ASSISTANT PROFESSOR/EEE, JAY SHRIRAM GROUP OF INSTITUTIONS, TIRUPUR

[2]PG SCHOLAR/ME-PED, JAY SHRIRAM GROUP OF INSTITUTIONS, TIRUPUR

***Abstract*—This paper represents the effective power management strategy to meet the demand of the remote area load based on wind, solar, hydrogen and diesel generator. For active power management, a hydrogen-based generation scheme consisting of an electrolyser and a fuel cell system is integrated to the RAPS system. In addition, the requested energy by the residential appliances presents random behavior, which can be lower or higher than the produced energy from the renewable sources. Using the wind turbine and the PV power generation system with the energy storage will reduce the fluctuations of the wind power and the load ones. The energy storage system requires capital investment; thus, it is important to estimate the reasonable storage capacities without an overflow size for the desired applications. In addition, a good strategy for energy management is necessary to reduce the variation impacts of the wind energy and the load for the battery and the residential appliances.**

Index Terms*—Current control, dc/dc converters, diesel generator, energy management, lithium battery, maximum power point tracking (MPPT), micro grid, photovoltaic (PV) panel, polynomial controller, ultracapacitors (UCs), wind turbine.

I.INTRODUCTION

During the next decade, micro grids will emerge as a major enabler of the smart grid for the integration of small and medium-sized distributed energy resource (DER) units into the electricity grid. Micro grids offer a promising cost-effective Solution for the integration of renewable energy with reduced losses, lower transmission and distribution costs, higher energy efficiency, and a number of environmental and economic benefits. However, the coexistence of multiple energy resources with differing dynamic properties has raised concerns over the stability, control, and efficiency of micro grids. The control and operation of micro grids are challenging, especially during islanded mode due to no or low inertial, dispatchable and non-dispatchable, and non firm characteristics of DER units.

These characteristics of DER units might give rise to load-tracking problems in the islanded mode of micro grid operation. The ac bus of the hybrid grid has the advantage of utilizing the existing ac system infrastructure, whereas the efficiency, size, and cost of a dc micro grid can be significantly improved because of less power conversion stages and of being transformer less .The coexistence of both ac and dc micro grids can merge the advantages of individual ac or dc micro grids to reach system operating efficiency that can never be attained by any single micro grid or DG.

It is obvious that grid-integrated WECS should generate at constant electrical frequency, determined by the grid. However, it is advantageous to vary the mechanical speed of the turbine/generator to maximize power capture with fluctuating wind velocities. Therefore, WECS is a classic example of a variable speed constant frequency (VSCF) system. Rotor side control of a grid-connected wound rotor induction machine is very attractive for such VSCF application, particularly when the speed range is limited. With a suitable integrated approach toward design of a WECS, use of a slip-ring induction generator is economically competitive, when compared to a cage rotor induction machine. The higher cost of the machine due to the slip rings is compensated by a reduction in the sizing of the power converters. The generator rating can also be reduced compared to other singly fed machines.

A d-q reference frame aligned with the stator flux is used for rotor current control. Indirect control of stator voltage is achieved by regulating the stator flux via the d-axis rotor current whereas the q axis rotor current is controlled to assure correct orientation of the reference frame. Sub and super synchronous operation is made possible by using two PWM conveners between the stator and the rotor. These converters are rated only for a fraction of the WEC system power. The stator side convener operates as a unity displacement factor hi-directional rectifier and regulates the DC link

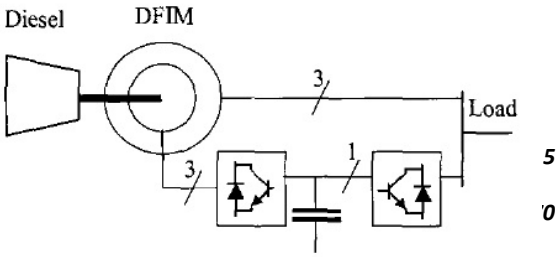

voltage. Constant stator frequency, with varying rotor speed, is achieved by using the rotor side converter to impose rotor currents of an appropriate frequency. Minimum fuel consumption of the diesel, for any given load, is obtained by regulating the speed to follow an optimum operating curve.

Fig. 1 System Schematic

Constant speed constant frequency (CSCF) WECS using cage rotor induction machine are most widely used because of their design simplicity and low cost. Variable speed systems with cage rotor induction generators are also commercially available, where energy output can be substantially improved and unity power factor operation is possible. A grid-connected doubly fed induction generator is an interesting option with a growing market demand and presently, research is active on the various control aspects for VSCF application. Vector control or direct torque control methods have been successfully employed to control the active and reactive powers handled by the generator. Although the individual technologies are well reported, so far a comparative study of these systems is not available.

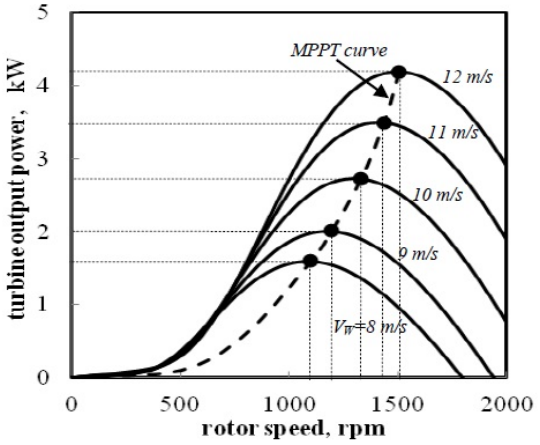

Fig. 2 Wind turbine output power curve for various wind velocities

In this paper, a VSCF system using wound rotor induction machine is compared against the existing fixed speed and variable speed systems using cage rotor machines on the basis of

i) Major hardware components required
ii) Operating region,
iii) Energy output due to a defined wind function.

This exercise clearly brings out the superiority of the doubly fed induction machine in terms of generator sizing, generated energy and the cost of power electronics involved.

II. MULTISOURCES AND DC/DC CONVERTERS MODELING

A. DGS Operation Principle

Where the wind turbine and the PV are used to inject the produced power in the dc-bus without the

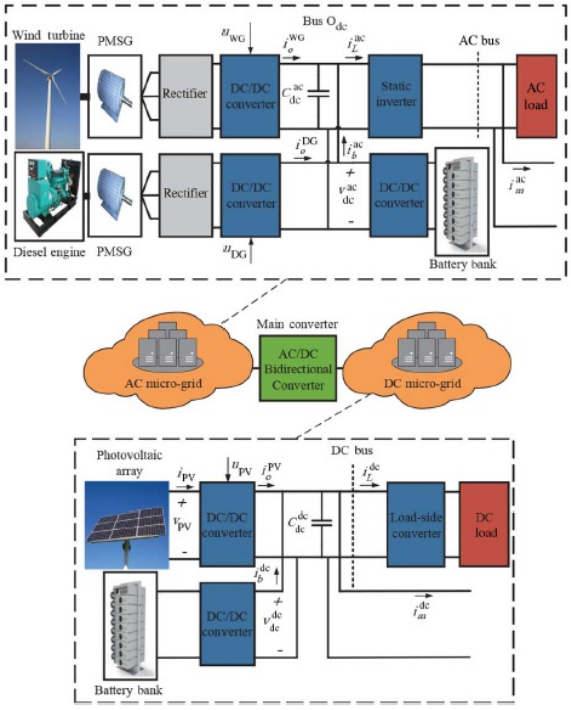

energy production optimizing the meaning of the classical maximum power point tracking (MPPT). The main goal is obtaining the fluctuating power according to the wind and the load variations. The Lithium battery and the UCs are added to the system to compensate the fluctuating power from the wind turbine and the load. Due to the energetic autonomy problem, a diesel generator is used for energy production if there is not enough power from the generation and the storage devices to cover the load. In addition to this role, the diesel generator is used for dc-bus voltage control when the wind turbine and the PV inject the power in dc-bus. Thus, energy management in the whole system can be reduced to current control, as illustrated.

Fig. 3 Typical hybrid ac/dc micro-grid Configuration

B. AC Micro-Grid Modeling

As seen in Fig. 3, the ac micro-grid is based on a DG and a WG working in parallel. The wind subsystem includes a windmill, a multipolar permanent magnet synchronous generator (PMSG), a rectifier, and a dc/dc converter. It should be noted that the power generated by wind turbine is controlled through a dedicated dc/dc converter. The mechanical output power of the wind turbine can be calculated as

$$P_m^{WG} = \tfrac{1}{2}\, Cp(\lambda)\rho A v3\ \text{wind} \quad (1)$$

Where $Cp(\lambda)$ is performance coefficient of the turbine and is modeled as $Cp(\lambda) = C1(C2/\lambda i - C3)e^{-C4/\lambda i} + C5\lambda$, in which $1/\lambda i = 1/\lambda - 0.035$, C1 = 0.5176, C2 = 116, C3 = 5, C4 = 21,C5 = 0.0068.
It is well known that the efficiency of a diesel engine depends on the operating speed and output power of the engine. However to improve the fuel efficiency and reduce emission, the diesel engine speed can be adjusted according to the load conditions. For this purpose, a variable speed diesel engine, a PMSG, a rectifier, a dc/dc converter, and an inverter are implemented as shown in Fig. 3, in which the power generated by the DG is controlled through the corresponding dc/dc converter. The transfer function of the model of prime mover is

$$P^{DG}m\ /Idiesel = kpm\ /\tau pms + 1e^{-tds} \quad (2)$$

In the proposed system, MPPT algorithm is developed employing P&O method. As the dc grid voltage is fixed, variation in wind output power results in variation of the dc current (i.e., output current of the dc-dc converter) fed to the dc micro grid. Therefore, the controller senses this dc grid current through a current sensor and compares it with the previous value.

C. DC Micro-Grid Modeling

The dc micro-grid, as shown in Fig. 3, comprises a PV array connected to the dc bus through a dc/dc converter, which controls operating point of the array. Generated current by the PV array is

$$iPV = npIph - npIrs(e^{qvPV/\,nsBKTc} - 1) \quad (4)$$

Many methods are presented in the literature based on the MPPT techniques, which are generally used with dc/dc converters for PV applications.The wind and solar sources are generating power together in this case, and the variation of the duty cycle of the dc–dc converter will eventually disturb the PV array's terminal voltage (since VDC = VPV). The rectifier voltage varies with the wind speed, and the duty cycle of the boost converter needs to be automatically adjusted such that *V*DC is equal to the peak power point voltage (Vm) of the PV array. At this point (VPV = VDC = Vm), the PV array delivers the maximum current (Im) which is concurrently drawn by the current-controlled inverter. To operate the PV array at its maximum power point (A), the dc–dc converter output (dc link voltage) is adjusted to Vm by varying the duty cycle of the dc–dc converter by controller.

The duty cycle variation of controller is given by

$$\delta new = \delta old + sgn(\Delta P)sgn(\Delta VPV)\Delta\delta \quad (5)$$

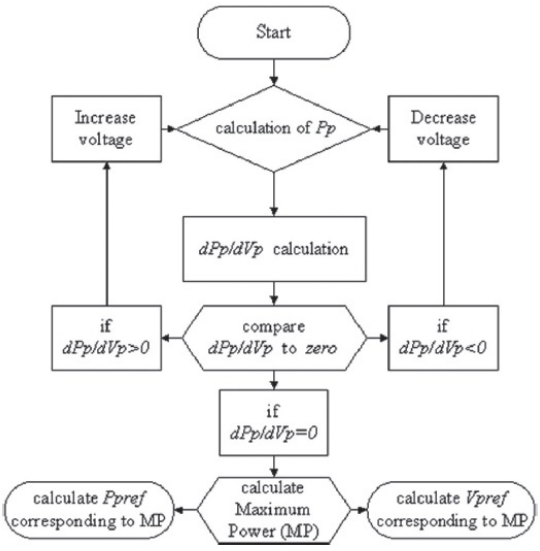

Fig. 4 Extraction method of the maximum power *P*pref and the corresponding voltage *V*pref

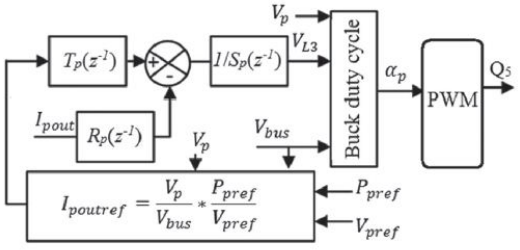

Fig. 5 PV current control loop

To control the power delivered by the PV panels, the polynomial control method is also used, as illustrated in Fig. 5, where *P*pref and *V*pref are obtained from Fig. 4. In order to obtain a minimal static error with disturbance rejection, the *Rp*(*z*−1), *Tp*(*z*−1), and *Sp*(*z*−1) polynomial correctors are selected similar to that presented in system. The polynomial coefficients obtained from closed-loop analysis are presented in system, where *L*3 is the current smoothing inductance and *ωp* is the current control bandwidth, i.e.,

$$\begin{cases} r0\ p = 2^* (1 - \exp(-\omega p\ ^*Te)) * L3/Te \\ \omega p = \log(2) * \chi p/Te \\ r1\ p = (\exp(-2 * \omega p * Te) - 1) * L3/Te \end{cases} \quad (6)$$

The buck converter control law is given as

$$\alpha p = Vp + VL3/V\text{bus} \quad (7)$$

This control law is used for Q5 PWM signal generation, as presented in Fig. 5. The functions always to feed the maximum power either from both sources or from any one of the sources to the grid by adjusting Iref. On the other hand, controller is idle when power is generated by PV alone.

III. ENERGY MANAGEMENT IN THE DGS BASED ON THE FREQUENCY APPROACH

The main goal of this paragraph is to establish the dc/dc converter control laws for energy management between the sources and the load (requested energy in the building) by taking into account the dynamic behavior of the sources.

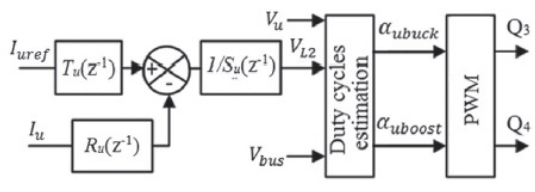

Fig. 6. HFC (UC current) control loop

A. HFC and LFC Control Method

The proposed control method for the HFC allocation to UCs is based on the polynomial control technique. This control method is presented in Fig. 6. In order to obtain a minimal static error with disturbance rejection, the Ru(z−1), Tu(z−1),and Su(z−1) polynomial correctors are selected, as expressed in the following equation:

$$\begin{cases} Su(z^{-1}) = 1 - z{-}1 \\ Tu(z^{-1}) = Ru(z^{-1}) = r0u + r1u * z^{-1} \end{cases} \quad (8)$$

The final coefficients of the polynomial correctors, which were obtained from closed-loop analysis, are presented for the UC current management, i.e.,

$$\begin{cases} r0u = 2^* (1 - \exp(\omega i\ ^*Te)) * L2/Te \\ \omega i = \log(2) *\ \chi i/Te \\ r1u = (\exp(-2 * \omega i * Te) - 1) * L2/Te \end{cases} \quad (7)$$

In this equation, *L*2 presents the UC current smoothing inductance, *Te* is the sampling period, and ωi is the current control bandwidth. The χi parameter is introduced in ωi, as illustrated. This variable is selected between ranges, and it gives many possible values of the bandwidth to optimize the performance of the control. It is estimated during real-time operations from a potentiometer connected to microcontroller's analog-to-digital conversion channel. The control laws for the buck-and-boost converter in the UC side, where *α*ubuck corresponds to buck mode, and *α*uboost is the boost converter control law, i.e.,

$$\begin{cases} \alpha\text{ubuck} = Vu+VL2\ /\ V\text{bus} \\ \alpha\text{uboost} = 1- Vu-VL2\ /\ V\text{bus} \end{cases} \quad (8)$$

These control laws are compared with a triangular waveform to generate Q3 and Q4 signals (Pulse width modulation) for the UC current management, as presented in Fig. 6. The allocation method of the LFC to the lithium battery is the same as that of the UC; that is why it is not necessary to present this last one. The same control loop is used to generate Q1 and Q2 for the lithium-battery's current management.

B. HFC and LFC Extraction Method

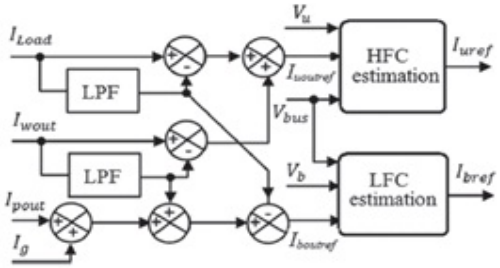

The wind/load variations cause some micro cycles for the energy storage devices, which include the HFC and the LFC. These components are not adapted to separate the electrical performances of the battery and the UCs. In other terms,

Fig. 7 HFC and LFC extraction method

Using only the battery to meet these micro cycles decreases its lifetime, and using the UCs without the battery to meet these micro cycles increases the UC size and cost. Based on electrical performances of the UCs and the battery, the UCs present high dynamic performances in terms of the charge/discharge cycle, and their lifetime is about ten years higher than that of the battery.

Moreover, the UCs have a power density from 10 to 100 times larger than that of the battery with an energy density much smaller; this is why it is necessary to combine the battery and the UCs to compensate the fluctuating power.

To reduce the impacts of the micro cycles for the battery and the micro grid, the authors propose the energy management strategy based on the frequency approach, which consists to allocate the HFC to UCs and the LFC to the battery.

C. Current Controller

IPV and Ib are sensed by the current transducers and digitized by the internal ADC module of the microcontroller. Iref is determined and available as a digital output from the microcontroller. This digital value is subsequently processed by a digital-to-analog conversion IC to obtain a dc value which corresponds to the peak value of Iref . This dc value is multiplied with the sine wave reference extracted from the grid voltage by a multiplier IC and fed to the hysteresis current controller as the reference current signal. When the PV array (or PMSG) alone generates power, Ib (or IPV) will be zero, and Iref is perturbed and adjusted automatically to extract the maximum power from the PV array (or PMSG).

When both sources are generating, Iref will be perturbed based on (15) and adjusted to maximize the dc-link current *I*DC for the corresponding irradiation and wind speed conditions. As the sine wave reference is taken from the grid.

D. Wind Energy System Control Strategy

The considered system is based on a wind turbine emulator coupled to a PMSG. Wind energy is converted to dc form using a three-phase diode rectifier. The output of this last one is connected to the buck converter to extract the maximum power available from the wind energy system. The extracted maximum power is injected in the dc-bus, and it presents the fluctuating components according to the wind speeds, which necessitate some compensation. To compensate these fluctuations, the UCs and the battery are used. The estimated maximum power of the wind turbine is expressed as follows:

$$Pwmax \approx (9/4*p/\pi * \phi 2f/ Ls)* \lambda opt/rt* v \quad (9)$$

Where λopt is the tip speed ratio fixed to 5.7, and *v* is the wind speed (in m/s). This maximum power is used to estimate the *I*woutref reference current, as illustrated. To control the power delivered by the PMSG, the polynomial control method is also used. In order to obtain a minimal static error with disturbance rejection, the Rw(z−1), Tw(z−1), and Sw(z−1) polynomial correctors are selected similar The polynomial coefficients obtained from closed-loop analysis are presented in the following equation, where L4 is the Iwout current smoothing inductance and ωw is the Iwout current control bandwidth:

$$\begin{cases} r0w = 2* (1 - \exp(-\omega w *Te)) *L4/Te \\ \omega w = \log(2) * \chi w/Te \\ r1w = (\exp(-2 * \omega w *Te) - 1) * L4/Te \end{cases} \quad (10)$$

The control law for the wind energy management is presented as

$$\alpha w = Vw + VL4 / Vbus \quad (11)$$

IV. OPERATION OF PROPOSED SYSTEM

The proposed PMS, consists of a central unit, fed with the data collected from all micro-grid components, in order to determine efficient strategies for power flow between energy resources. The input variables to the ROPMS are generation forecast (Pmax WG , Pmax PV), demanded power (Pac *D* , Pdc *D*) (sum of load power, power line loss, and power loss due to the circulating current), SOC of the battery banks (SOCac, SOCdc), and some statistical and dynamical operational limits. It is noteworthy that some of the operational limits are constant through

the ROPMS operation, such as minimum generation capacity of solar and wind subsystems (Pmin PV, *P*min WG), minimum and maximum generation capacity for the DG (Pmin DG , *P*max DG), maximum allowable power exchange between the ac and dc micro-grids (Pmax ac2dc, Pmax dc2ac), the minimum amount of time for which the DG must be kept ON, maximum allowable changing rate of the battery bank outputs (ΔPac rate,ΔPdc rate), and minimum and maximum SOC of the battery banks (SOCmin, SOCmax).

A . Lithium-Battery Modeling

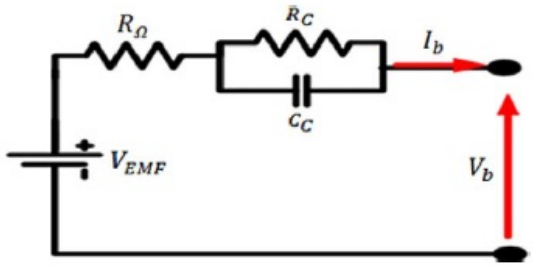

Fig. 8 Lithium-battery dynamic model

TABLE I
LITHIUM-BATTERY PARAMETERS

DESCRIPTION	SYMBOL	VALUE	UNIT
Open circuit voltage	VEMF	20.15	V
Series resistance	RΩ	94.2	mΩ
Polarization resistance	RC	73.6	mΩ
Equivalent resistance	CC	4581	F

The used model of the lithium battery is presented in Fig. 8. This model includes an open circuit voltage *V*EMF, which is according to the state of charge; an internal resistance *R*Ω; and a parallel *RC* circuit, which describes the charge transfer and the diffusion process between the electrode and the electrolyte. The lithium-battery analytical model is presented in the following equation,

$$V_b = V_{EMF} - (R_\Omega + R_C/1 + C_C * R_C * S) * I_b \quad (12)$$

Fig. 9. Determination algorithm

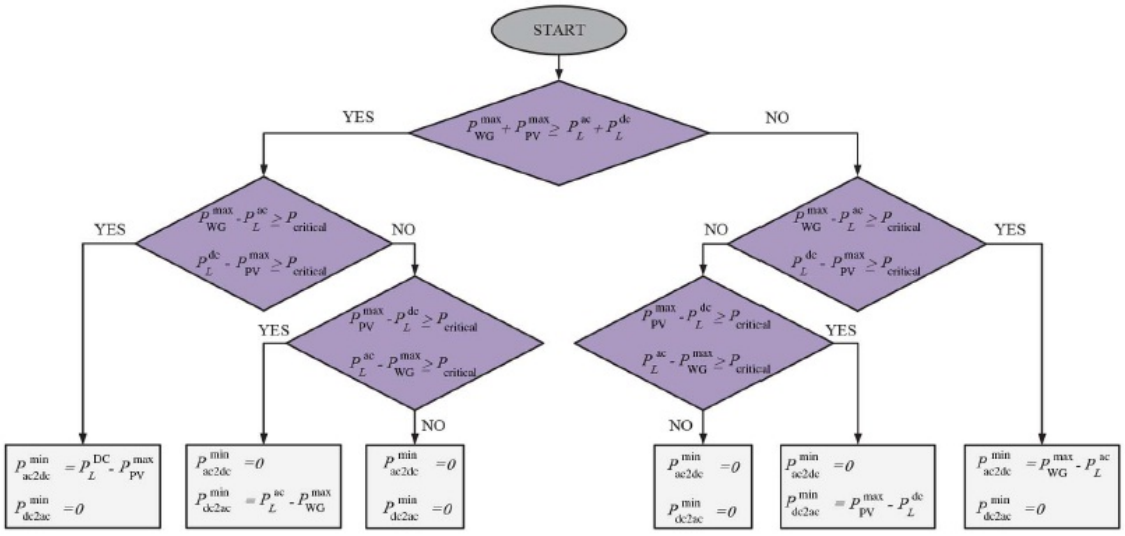

B. Operational Limits Computation

When the dc micro-grid injects power to the ac micro-grid, the ac power is obtained from two parallel connected dc/ac converters. On the other hand, when the ac micro-grid injects power to the dc micro-grid the main converter acts as an ac/dc converter.

Thus, dc power is obtained from two parallel-connected converters:

The dc/dc converter of the solar subsystem and the main converter. In both cases, it is shown that even small mismatches between the output voltages of the converters could increase power

loss due to the circulating current and damages the power semiconductors, which are referred to as "conversion quality" in this paper. Nevertheless, forcing the micro-grids to work independently may lead to not utilizing maximum available wind or solar power and may hamper the efficiency of the system. Hence, a tradeoff between the conversion quality and system efficiency should be considered to determine the amount of power which can be exchanged between the micro-grids.

In this algorithm, when the total available power is more than the total power demand, and also unexploited power in ac micro-grid and power shortage in dc micro-grid are more than a critical value (Pcritical), the ac micro-grid feeds the required power into the dc micro-grid. Hence, Pmin ac2dc is set to the power shortage in the dc micro grid. Also, when unexploited power in dc micro-grid and power shortage in ac micro-grid is more than Pcritical, the dc micro grid supplies power shortage in the ac micro-grid and Pmin dc2ac is equal to power shortage in the ac micro-grid. Now, suppose that total available power is less than total power demand. In this case, when unexploited power in ac micro-grid is more than *P*critical, the ac micro-grid injects the unexploited power to the dc micro-grid, and then Pmin ac2dc is equal to the unexploited power in ac micro-grid. Also, when unexploited solar power is more than *P*critical, the dc micro-grid injects power to the ac micro grid. In this case, Pmin dc2ac is set to the unexploited solar power in the dc micro-grid.

The value of Pcritical specifies the attitude of the proposed algorithm toward the considered tradeoff. Small values of *P*critical prioritize utilizing maximum available power, and consequently increase the system efficiency. However, small values may increase the power loss due to the circulating currents, and may lead to damage of the power semiconductors. On the other hand, high values of Pcritical, although prioritize achieving high conversion quality, it may hamper the efficiency of the system.

In all of the aforementioned hybrid DG systems with PMSG–PV attempted so far, the system had either individual power converters for each of the sources or a battery backup. Furthermore, each converter was controlled using complex algorithms for peak power tracking. In order to minimize the conduction and switching losses of the devices, it is necessary to have the minimum number of power converters (power conversion stages), and this has been attempted in this paper.

In addition, it is desirable that power supplies in consumer sites employ fewer power electronic conversion stages in order to improve the overall efficiency. It should be noted that losses in conversion stages have to be compensated by increasing the sizes of the generators. This, in turn, increases the cost of the hybrid generator. Generally, the efficiency of a dc–dc converter is maximum around 95% when it is operated in full load condition. Since source powers are varying, it is not always possible to operate the dc–dc converter at its maximum efficiency. In the aforementioned context, the proposed new topology avoids 5% loss in efficiency by eliminating an additional conversion stage.

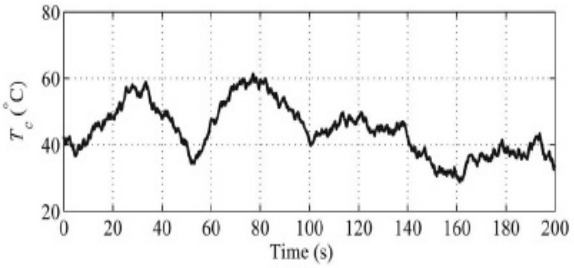

Contrary to earlier schemes, the proposed hybrid generator has a PV array being directly connected to the dc link instead of being connected through a dc–dc converter. The dc-link voltage is varied by a dc–dc converter interposed between the rectifier fed by the PMSG and the grid-connected inverter.

The output voltage of the dc–dc converter forms the load line for the PV array. The inverter current is varied to extract the maximum current from both sources using current control strategy. The proposed topology could thus dispense with a dc–dc converter, which, in earlier schemes, was connected after the PV array for maximum power extraction.

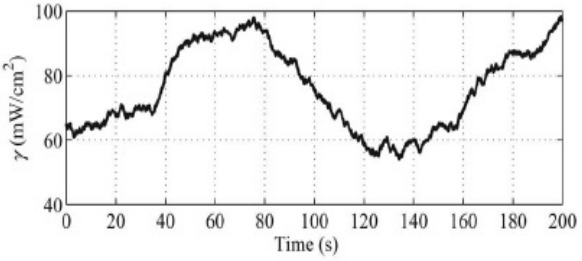

V. SIMULATION RESULTS

To validate the proposed control methods for the decentralized energy generation systems focused on the renewable energy sources, the dc-bus voltage reference is fixed to rated voltage using a

controlled dc-source. The proposed system has also been simulated using Sim Power Systems toolbox in MATLAB software. The same machine considered in the earlier section along with other parameters has been used for the simulation.

Fig 10. Wind speed

Experimentally obtained magnetization characteristic (current versus voltage) of the induction machine at rated frequency of 50 Hz with a constant speed of 1500 rpm has been used in the asynchronous machine model available in the MATLAB.A 3-phase DBR along with the dc-dc converter has been built using the components available in the MATLAB and this has been connected in between the generator output terminals and dc grid. A WT model available in the MATLAB has been used to drive the induction generator. WT model gives the mechanical torque as output for a given wind velocity. This torque has been given as input to the induction machine model as a negative value for generator operation. PMSG contribution in the dc-bus that corresponds to the maximum power extracted from the wind turbine.

Fig 11. Cell temperature

Fig 12. Solar radiation

The PV panels provide the maximum power to the dc-bus. During the online operations, the experimental current from PV panels presents some ripples due to variations of the sun. Contrary to the experimental result, the simulation curve has no ripples due to solar irradiation, which is considered constant for the simulations. The fluctuations of the PMSG power due to wind variations can be assigned to the Iwout current because the dc-bus voltage is constant.

Fig 13. Maximum available power

The injected current in the dc-bus from the PMSG, which corresponds to the extracted maximum power from the wind turbine. This current presents many fluctuations, which are not adapted to the load's request.

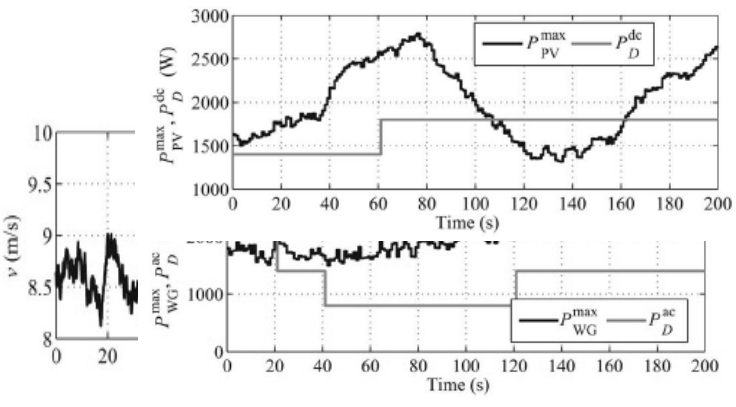

Fig. 14 Demand power

A. Dynamic performance

To validate the satisfactory dynamic performance of the proposed system with the MPPT controller, simulation has also been carried out for step change in wind velocity. In this simulation, wind velocity has been changed from 8 m/s to 10 m/s and back.

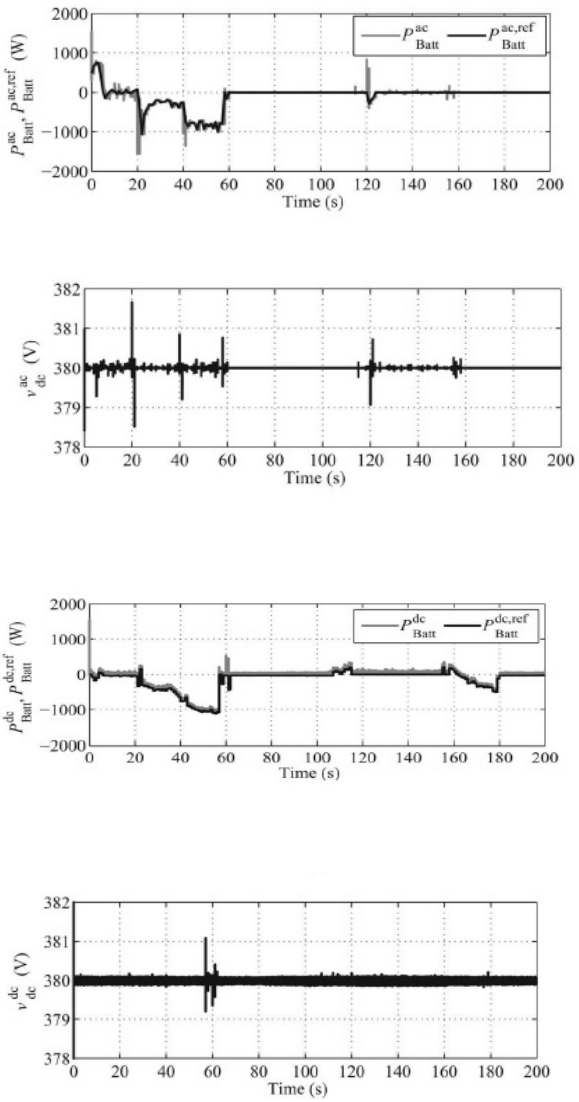

Fig. 15 Simulation results showing the effectiveness of the proposed two-level scheme on regulating the voltage level.

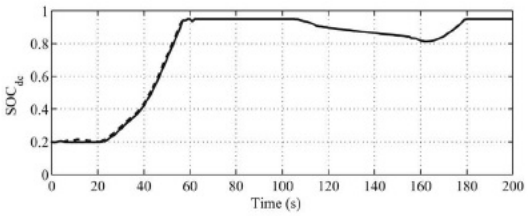

Fig. 16 Simulation results showing the effectiveness of the ROPMS on minimizing the DG operation.

Simulations have also been carried out by increasing the duty ratio with increasing dc grid current for the step change in wind velocity from 8 m/s to 10 m/s and back. All the waveforms given in Fig. 6 have also been observed for this setting and noted that the controller settled with the operating point similar to the 'point B' mentioned in Fig. 5. Further, to assess the successful working of the proposed MPPT algorithm for large value of inertia of WT system as compared to the results furnished in Fig. 6, simulation has been carried out with J=0.075 kg.m2 retaining the other parameters same. For the sake of brevity, simulated results of only *Nr*, *Tm*, *Te*, *Pe*, *Idc* and *Pdc*.This result further confirms the satisfactory working of the proposed MPPT algorithm even for the large value of inertia of WT system.

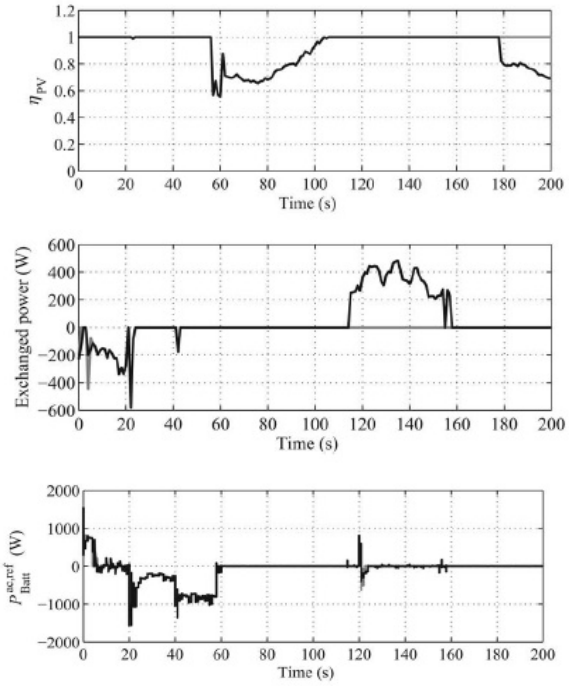

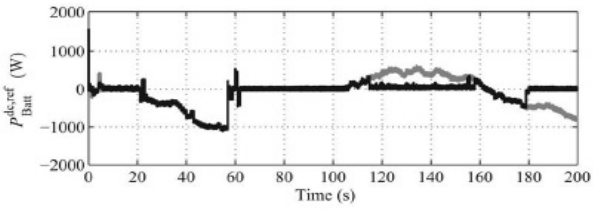

Fig. 17 Simulation results showing the effectiveness of the proposed algorithm on increasing the efficiency.

When the PMSG shaft speed had increased, the PMSG output power also had correspondingly increased and the current reference generated by controller also had increased proportionally in order to extract the available maximum power. As the dc motor speed increases, the input voltage to the dc–dc converter also increases, and hence, the duty cycle of the boost converter automatically decreases to maintain the dc-link voltage to the PV's maximum power point voltage.

In order to further ascertain the operation of the controller in tracking the peak power from both sources, the simulated peak power available and the peak power extracted from the theoretical results were compared for various conditions. Close conformity of the experimental peak powers with the simulated peak powers of both sources under varying wind speed (PMSG shaft speed) and irradiation (*I*SC) confirms adequately the successful operation of the controllers.

The total harmonic distortions (THDs) of the voltage and the current at the grid side were measured by using a analyzer block in simulation. It can also be noted that the voltage and current THDs are 1.8% and 4.6%, respectively, which are below the allowable THD recommended by IEEE for interconnecting distributed resources with utility.

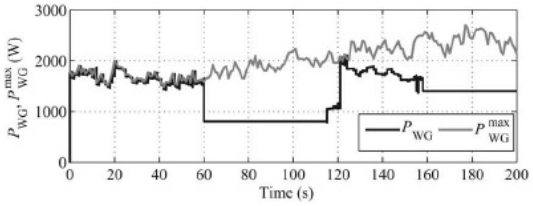

Fig. 18 Simulation results showing the robustness of the proposed RAPS in case of generation estimation errors.

B. Comparison of the System Cost for Different Cases

Finally, different cases are studied with regard to the system cost. Here, first case corresponds to the normal operation of the micro-grid without any uncertainty, Second case Corresponds to the condition in which no penalty is considered for the output power of the DG, Third case corresponds to the condition in which generation forecasts are uncertain, and Fourth case corresponds to the condition in which output power of the generation systems are uncertain. For each case, the system costs are computed at each sampling instant ($F(k)$, $k = 1, \ldots, 200$), and their statistics such as minimum, maximum, mean, standard deviation (SD) and total cost (TC).

The high system cost of the second case is mainly because of the high cost assigned to the DG operation. As stated in sections the presence of generation forecast errors, robustness is ensured at the cost of losing optimality, i.e., although the proposed ROPMS can treat the generation forecast errors, the proposed optimization problem will return a suboptimal solution. Where the system cost for third case is higher than that of first case. In this paper, a two-level control scheme is proposed to regulate the charge/discharge power of the battery banks to compensate the power imbalances caused by the output power uncertainties. Output power uncertainties can affect the system cost. However, its effect is less than the effect of the uncertainties in the estimated maximum available solar and wind powers.

IV. CONCLUSION

A new reliable hybrid DG system based on PV and wind driven PMSG as sources, with only a boost converter followed by an inverter stage, has been successfully implemented. The mathematical model developed for the proposed DG scheme has been used to study the system performance in MATLAB.

The investigations carried out in a laboratory prototype for different irradiations and PMSG shaft speeds amply confirm the utility of the proposed hybrid generator in zero-net-energy buildings. In addition, it has been established through experimentation and simulation that the two controllers, digital MPPT controller and hysteresis current controller, which are designed specifically for the proposed system, have exactly tracked the maximum powers from both sources.

Maintenance-free operation, reliability, and low cost are the features required for the DG employed in secondary distribution systems. It is for this reason that the developed controllers employ very low cost microcontrollers and analog circuitry. Furthermore, the results of the experimental investigations are found to be matching closely with the simulation results, thereby validating the developed model. The steady state waveforms captured at the grid side show that the power generated by the DG system is fed to the grid at unity power factor.

The voltage THD and the current THD of the generator meet the required power quality norms recommended by IEEE.

REFERENCES

[1] D. F.Warne, “Generation of electricity from the wind,” Proc. Inst. Elect.Eng., vol. 124, pp. 963–985, Nov. 1977.

[2] C. V. Nayar, “Wind power—The near term commercial renewable energy source,” Australi. Sci., Summer Issue, vol. 16, no. 4, pp. 25–26,1995.

[3] Getting Connected—Integrating Wind Power With Electric Utility Systems,” Rep. Ameri. Wind Energy Assoc., 1997.

[4] A. Miller, E. Muljadi, and D. S. Zinger, “A variable speed wind turbine power control,” IEEE Trans. Energy Conversion, vol. 12, pp. 181–187, June 1997.

[5] S. A. Daniel and N. A. Gounden, “A novel hybrid isolated generating system based on PV fed inverter-assisted wind-driven induction generators, ”*IEEE Trans. Energy Convers.*, vol. 19, no. 2, pp. 416–422, Jun. 2004.

[6] H. Polinder, F. F. A. van der Pijl, G. J. de Vilder, and P. J. Tavner, “Comparison of direct-drive and geared generator concepts for wind turbines,” *IEEE Trans. Energy Convers.*, vol. 21, no. 3, pp. 725–733, Sep. 2006.

[7] C. N. Bhende, S. Mishra, and S. G. Malla, “Permanent magnet synchronous generator-based standalone wind energy supply system,” *IEEE Trans. Sustain. Energy*, vol. 2, no. 4, pp. 361–373, Oct. 2011.

[8] H. C. Chiang, T. T. Ma, Y. H. Cheng, J. M. Chang, and W. N. Chang, “Design and implementation of a hybrid regenerative power system combining grid-tie and uninterruptible

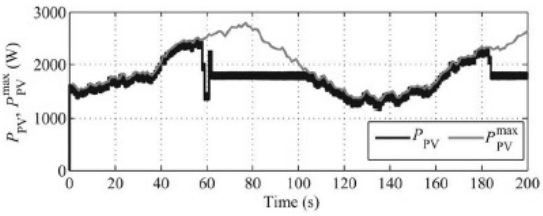

power supply functions," *IET Renew. Power Gen.*, vol. 4, no. 1, pp. 85–99, 2010.

[9] S.-K. Kim, J.-H. Jeon, C.-H. Cho, J.-B. Ahn, and S.-H. Kwon, "Dynamic modeling and control of a grid-connected hybrid generation system with versatile power transfer," *IEEE Trans. Ind. Electron.*, vol. 55, no. 4,pp. 1677–1688, Apr. 2008.

[10] F. Giraud and Z. M. Salameh, "Steady-state performance of a grid connected rooftop hybrid wind-photovoltaic power system with battery storage," *IEEE Trans. Energy Convers.*, vol. 16, no. 1, pp. 1–7, Mar. 2001.

[11] S. Bae and A. Kwasinski, "Dynamic modeling and operation strategy for a micro grid with wind and photovoltaic resources," *IEEE Trans. Smart Grid*, vol. 3, no. 4, pp. 1867–1876, Dec. 2012.

[12] Y.-M. Chen, Y.-C. Liu, S.-C. Hung, and C.-S. Cheng, "Multi-input inverter for grid connected hybrid PV/wind power systems," *IEEE Trans. PowerElectron.*, vol. 22, no. 3, pp. 1070–1077, May 2007.

[13] L. Xu, and D. Chen, "Control and operation of a DC microgrid with variable generation and energy storage," *IEEE Trans. Power Del.*, vol. 26, no. 4, pp. 2513–2522, Oct. 2011.

[14] J. Lago and M. L. Heldwein, "Operation and control-oriented modeling of a power converter for current balancing and stability improvement of dc active distribution networks," *IEEE Trans. Power Electron.*, vol. 26, no. 3, pp. 877–885, Mar. 2011.

[15] A. Yazdani and P. P. Dash, "A control methodology and characterization of dynamics for a photovoltaic (PV) system interfaced with a distribution network," *IEEE Trans. Power Del.*, vol. 24, no. 3, pp. 1538–1551, Jul. 2009.

[16] H. Li and Z. Chen, "Overview of different wind generator systems and their comparisons," *IET Renew. Power Gener.*, vol. 2, no. 2, pp. 123–138, Jun. 2008.

[17] X. Lu, J. M. Guerrero, K. Sun, and J. C. Vasquez, "An improved droop control method for dc microgrids based on low bandwidth communication with dc bus voltage restoration and enhanced current sharing accuracy," *IEEE Trans. Power Electron.*, vol. 29, no. 4, pp. 1800–1812, Apr. 2014.

[18] H. Kakigano, Y. Miura, and T. Ise, "Distribution voltage control for dc microgrids using fuzzy control and gain-scheduling technique," *IEEE Trans. Power Electron.*, vol. 28, no. 5, pp. 2246–2258, May 2013.

[19] K. Kurohane, T. Senjyu, A .Yona, N. Urasaki, T. Goya, and T. Funabashi, "A Hybrid smart AC/DC power system," *IEEE Trans. Smart Grid*, vol. 1, no. 2, pp. 199–204, Sep. 2010.

[20] R. C. Bansal, "Three-phase self-excited induction generators: an overview," *IEEE Trans. Energy Convers.*, vol. 20, no. 2, pp. 292-299, Jun. 2005.